RSC Advances

ROYAL SOCIETY OF CHEMISTRY

www.rsc.org/advances

RSC Advances

Cite this: DOI: 10.1039/c0xx00000x

www.rsc.org/xxxxxx

Article

Effect of alkaline electrolytes on the charge storage capacity and morphology of porous layered double cobalt hydroxide-coated graphene supercapacitor electrodes

Montakan Suksomboon,[a] Patarachai Srimuk,[a] Atiweena Krittayavathananon, [a] Santamon Luanwuthi, [a] and Montree Sawangphruk*[ab]

Received (in XXX, XXX) Xth XXXXXXXXX 20XX, Accepted Xth XXXXXXXXX 20XX
DOI: 10.1039/b000000x

Although alpha-cobalt hydroxide (α-$Co(OH)_2$) with a layered double hydroxide (LDH) structure has been widely used as the supercapacitor electrode, the effect of alkaline electrolyte on the charge storage performance of the α-$Co(OH)_2$ has not yet been investigated. In this work, α-$Co(OH)_2$ was electrodeposited on reduced graphene oxide-coated carbon fiber paper (rGO/CFP) using a chronoamperometry at -0.5 V vs. Ag/AgCl. The effect of alkaline aqueous electrolytes to the performance of the α-$Co(OH)_2$/rGO/CFP electrodes was then investigated by means of scanning and transmission electron microscopies, X-ray photoelectron and absorption spectroscopies, and electrochemical techniques. It was found that the concentrated alkaline electrolytes (i.e., 3-6 M [OH-]) can strip off and/or deform the porous structure of the α-$Co(OH)_2$ deposited on rGO/CFP leading to poor charge storage capacity. 1 M [OH^-] was found to be a suitable electrolyte concentration providing high specific capacitance (1096 F g^{-1} at 1.8 A g^{-1}) without the deformation of the porous α-$Co(OH)_2$ structure after testing. Morphological and electrochemical analyses of the α-$Co(OH)_2$/rGO/CFP electrodes suggest that the effect of the alkaline electrolyte concentration plays a major role to the charge storage performance of α-$Co(OH)_2$-based supercapacitors.

1. Introduction

The supercapacitors store energy via two energy storage mechanisms. The first one is based on an electrostatic adsorption of ionic charges at the electrode-electrolyte interface so-called *electrochemical double layer capacitance* (EDLC). The double dielectric layer is less than 1 nm in thickness leading to high capacitance. In addition to EDLC, pseudocapacitors store faradaic charges (electrons) via a surface redox reaction or electrosorption.[1, 2] In principle, the pseudocapacitors exhibit higher energy density but lower power density than EDLC capacitors. Overall, the supercapacitors have high specific power (ca. 5-100 kW kg^{-1}) but low specific energy (ca. 0.5-15 Wh kg^{-1}) when compared with batteries (ca. 35-150 Wh kg^{-1}).[3, 4] Novel nanomaterials with high surface area-to-volume ratio, conductivity, and porosity then needed to address this problem.

Nanomaterials play a vital role in improving the charge storage capacity of both EDLC capacitors and pseudocapacitors. Graphene has been widely used and recognized as the high-performance electrode of EDLC capacitors.[5-7] Whilst, $Co(OH)_2$ nanostructures, known as inexpensive, nontoxic, and electrochemically active pseudocapacitor materials, have ultrahigh charge storage capacity due to a large interlayer spacing between its adjacent layers of $Co(OH)_2$.[8, 9] Anions can be moved in/out through the spacing of $Co(OH)_2$. $Co(OH)_2$ LDHs have been produced by various techniques such as hydrothermal, solvothermal, microwave, sonochemical, and electrodeposition techniques.[10, 11] Among them, the electrodeposition is of great interest since it is relatively simple, cheap, and scalable. Changing deposition variables such as electrolyte, deposition potential, temperature, and time can accurately control the surface microstructure of the deposits.[12-14] Importantly, the active materials produced by the electrodeposition can be directly exposed to the electrolytes leading to high specific activity at very diluted loading content.[15] Additionally, there is no need of other materials e.g. polyvinylidene difluoride (PVDF) binder and conductive carbon black typically used for the fabrication of energy storage electrodes. Note, the active materials can be buried by PVDF and carbon black particles leading to inactive surface area of the materials.

In addition, there is another important issue relating to the electrolyte used for the electrochemical evaluation of $Co(OH)_2$

supercapacitor electrodes. Different concentrations of KOH (1-6 M) were previously used without explanation in details why KOH has been used and which suitable concentration of alkali should be used leading to difficulty in the performance comparison of $Co(OH)_2$-based supercapacitors. In this work, the effect of two alkaline electrolytes i.e., KOH and NaOH with different concentrations (1-6 M) on the charge storage capacity and the morphological structure of α-$Co(OH)_2$ LDH was systematically investigated. Interestingly, it turned out for the first time in this work that at high concentrations e.g. 3-6 M KOH and NaOH, the electrolytes are rather corrosive, which can strip off and/or deform the porous structure of the α-$Co(OH)_2$ LDH electrodeposited on reduced graphene oxide (rGO)-coated carbon fiber paper (CFP)[6, 16]. On the other hand, the α-$Co(OH)_2$ electrode tested in 1 M NaOH exhibits high charge storage performance without morphology change.

2. Experimental

2.1 Chemicals and materials

Graphite powder (20-40 μm, Sigma Aldrich), ethanol (99.9%, QRec), hydrogen peroxide (30%, Merck), d(−)-fructose (99%, Sigma–Aldrich), potassium chloride (≥99.5%, Qrec), hydrochloric acid (37%, Qrec), cobalt (II) nitrate hexahydrate (99%, Qrec), sodium hydroxide (98%, Carlo Erba), 1-methyl-2-pyrrolidone (99.5%, Merck), sulphuric acid (≥98%, Qrec), sodium nitrate (99.0%, Ajax), polyvinylidene fluoride (PVDF, Mw 534000, Sigma Aldrich), sodium sulphate (99%, Carlo Erba), 1-methyl-2pyrrolidone (99.5%, Merck), and potassium permanganate (99%, Ajax Finechem) are of analytical grade. All solutions were made up using Milli-Q (ultrapure) water with a resistance of >18 MΩ cm at 25 ºC. CFP from SGL CARBON SE, Germany has a thickness of 400 μm and the electrical resistance of <12 mΩ cm^2.

2.2 Electrodeposition of α-Co(OH)₂ on rGO/CFP

The preparation details of rGO powders were previously reported by our group elsewhere.[16-18] The rGO dispersion in acetone (1 mg ml^{-1}) was coated on graphitized CFP by a simple spray coating technique (Paasche Airbrush Company, USA). The airbrush head used a coating pressure and temperature of 20 psi and 25 °C, respectively. The specific loading of rGO on the CFP was around 1 mg cm^{-2}. $Co(OH)_2$ LDH with the anion (NO_3^-) interlayer was then electrodeposited on the rGO/CFP electrode using a chronoamperometry at -0.5 V vs. Ag/AgCl in 0.1 M $Co(NO_3)_2$ in 0.5 M $NaNO_3$ for different electrodeposition time. The as-electrodeposited electrode was washed by Milli-Q water for 5 times and vacuum dried for 3 h.

2.3 Morphological, structural, and electrochemical characterizations

The morphology of the as-electrodeposited α-$Co(OH)_2$ materials was investigated using scanning electron microscopy (SEM) (Philips: XL30) and transmission electron microscopy (TEM) (EI Tecnai G^2, Eindhoven, The Netherlands). The structural characterization was X-ray diffraction (XRD) (Philips X'Pert). The XRD patterns were recorded on a diffractometer with CuKα radiation (λ = 1.5406 Å) and a graphite monochromator at 40 kV, 30 mA. Energy-dispersive X-ray spectroscopy (EDX) (Hitachi S-3400, Japan) was used for the elemental analysis of the as-prepared electrodes. X-ray absorption spectroscopy (XAS) was used to determine the oxidation state of Co in the as-electrodeposited $Co(OH)_2$ structure. X-ray photoelectron spectroscopy (XPS) was also used to characterize the as-electrodeposited α-$Co(OH)_2$. Electrochemical measurements of the as-prepared electrodes were carried out at room temperature (25 °C) using a standard three-electrode configuration comprising a platinum wire counter electrode, a Ag/AgCl reference electrode, and a working electrode. A Metrohm AUTOLAB potentiostat (PGSTAT 302N) with a 10-A booster made in Netherlands running NOVA (version 1.10.3) software was used.

3. Results and discussion

3.1 Morphological and structural characterization

Fig.1a-f show as-electrodeposited $Co(OH)_2$ films on rGO/CFP substrates produced for different electrodeposition time (1-40 min). The morphology of $Co(OH)_2$ here is in good agreement with that of alpha-phase layer double cobalt (II) hydroxide, α-$Co(OH)_2$.[19] The mechanism of the electrodeposition of the $Co(OH)_2$ consists of a reduction reaction of NO_3^- (1) and a following precipitation reaction (2);

$$NO_3^- + 7H_2O + 8e^- \rightarrow NH_4^+ + 10OH^- \quad (1)$$

$$Co^{2+} + 2OH^- \rightarrow Co(OH)_2 \quad (2)$$

When a potential of -0.5 V vs. Ag/AgCl finely tuned was applied to the working electrode (rGO/CFP), nitrate ions in the electrolyte can be reduced on the cathodic surface to produce hydroxide ions. The generation of OH^- at the cathode raises the local pH, resulting in the precipitation of $Co(OH)_2$ LDH with the anion (NO_3^-) interlayer at the rGO/CFP surface. The colour of $Co(OH)_2$ deposit is green, which is an optical appearance of α-$Co(OH)_2$ (see Fig. S2a of ESI).[13]

When the reactions (1) and (2) take places, α-$Co(OH)_2$ films with high porosity are found on the rGO/CFP (Fig. 1). The pore size of air voids is clearly decreased when increasing deposition time. Large $Co(OH)_2$ nanosheets with open pore structure are clearly seen at a deposition time of 10 min (Fig. 1d). At longer deposition time (e.g. 20 and 40 min), the morphology of the deposit becomes denser and the nanosheets found at 10 min disappears (see Fig. 1e-f and low-magnification SEM images in Fig. S3e-f of ESI). The denser morphology may limit the electrolyte diffusion. On the other hand at short deposition time (1-5 min), the deposits did not completely cover the rGO/CFP, which may lead to low capacity retention (See Fig. S3a-c of ESI). EDX of all as-electrodeposited samples was also carried out and the results showed that the deposits consist of Co, O, and C elements.

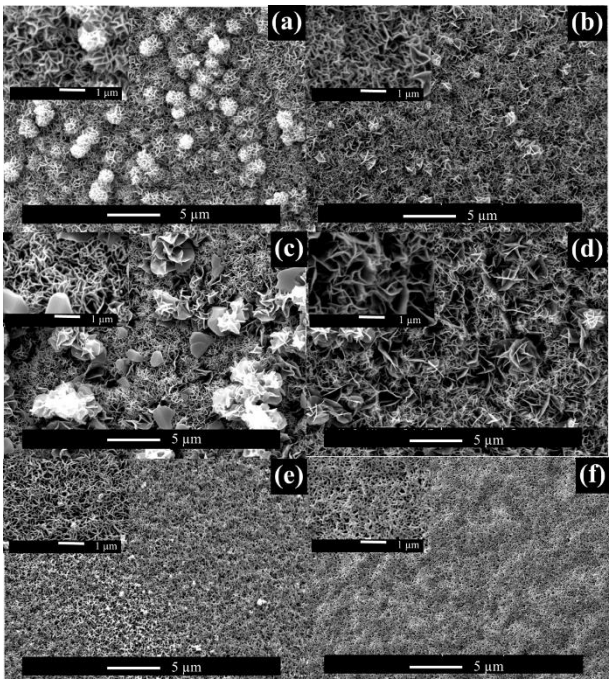

Fig. 1 SEM images of as-electrodeposited α-$Co(OH)_2$ on rGO/CFP electrodes using a chronoamperometry at -0.5 V vs. Ag/AgCl for different electrodeposition time; (a) 1 min, (b) 2 min, (c) 5 min, (d) 10 min, (e) 20 min, and (f) 40 min.

Fig. 2a and b show TEM images of rGO sheets and as-electrodeposited $Co(OH)_2$ on rGO sheets. A few layers of transparent rGO sheets overlap each other forming different surface morphologies (Fig. 2a). After the electrodeposition process, two-dimension (2D) $Co(OH)_2$ nanosheets are found on the rGO surfaces (Fig. 2b). The interfacial interaction between two layers is most possibly due to van der Waals force. The TEM result here is in good agreement with that of other LDHs (e.g. $Ni(OH)_2$) previously reported.[20] The EDX spectrum of $Co(OH)_2$/rGO is shown in Fig. 2c for which C, O, and Co elements are observed. Note, the Cu element is found due to the Cu grid used for the preparation of the TEM specimen. Fig. 2d shows the selected area electron diffraction (SAED) pattern of the $Co(OH)_2$ indicating the polycrystalline phase of $Co(OH)_2$ with two separated rings.[21]

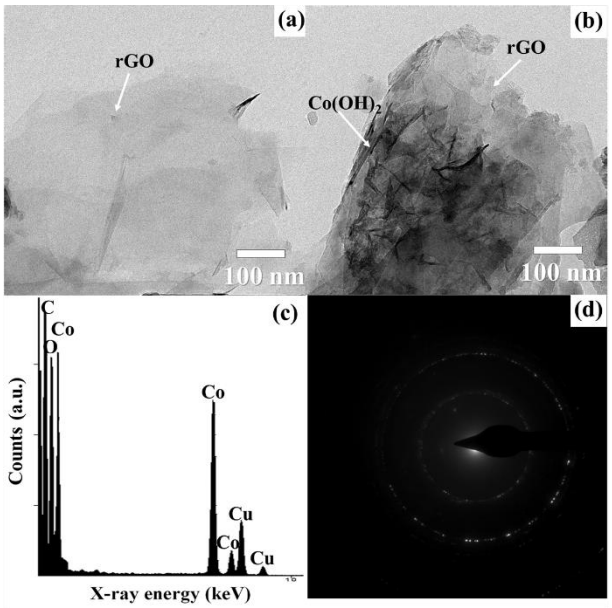

Fig. 2 TEM images of (a) rGO and (b) as-electrodeposited α-$Co(OH)_2$ on rGO sheets as well as (c) EDX and (d) selected area electron diffraction (SAED) pattern of α-$Co(OH)_2$.

$Co(OH)_2$ deposit was scrapped off from the electrode using a sharp doctor blade (see Fig. S2b of ESI). The powder XRD of as-scrapped $Co(OH)_2$ is shown in Fig. 3a for which all planes i.e., (003), (006), (012), (015), (018), and (110) are of α-$Co(OH)_2$.[22] The α-$Co(OH)_2$ with the nitrate anions in their spacing has a larger interlayer spacing (ca. 8.4 Å) than that of other phases e.g. β-$Co(OH)_2$ (4.6 Å).[22] As the result, the electrolytes may freely diffuse through the large spacing of α-$Co(OH)_2$.

XPS was carried out to confirm the structure of the as-electrodeposited α-$Co(OH)_2$ for which all XPS spectra were referenced to the aliphatic carbon at a binding energy of 285.0 eV. Wide-scan XPS spectra of rGO and as-electrodeposited α-$Co(OH)_2$/rGO/CFP are shown in Fig. 3b for which Co2p, C1s, and O1s are found on the samples confirming the EDX results. Fig. 3c shows a narrow-scan XPS spectrum of Co2p of the as-electrodeposited $Co(OH)_2$. Co2p spectrum exhibits a spin-orbit splitting into $Co2p_{1/2}$ and $Co2p_{3/2}$ components with a spitting energy of 16.2 eV. Both components can give the same quantitative information; thus, in this work the higher intensity $Co2p_{3/2}$ bands were only curve–fitted and the results in Fig. 3c show that a major peak at a binding energy of 780.4 eV is due to Co^{2+} of $Co(OH)_2$ and minor peaks are due to shake-up satellite effect. This result is in good agreement with other previous work.[23, 24]

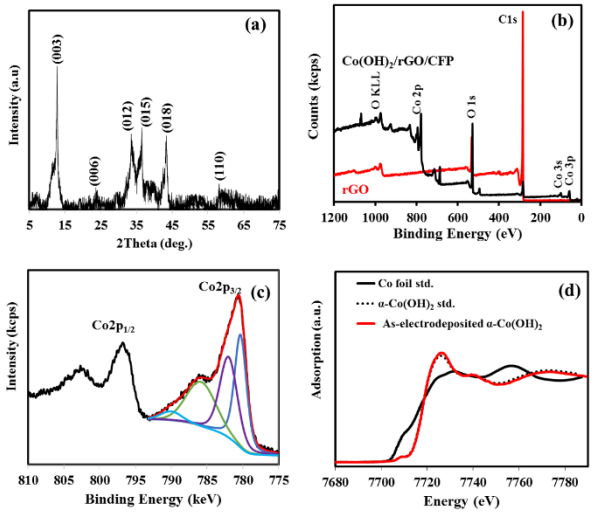

Fig. 3 (a) XRD pattern, (b) wide scan XPS, (c) narrow scan XPS spectra, and (d) XAS spectra of as-electrodeposited α-$Co(OH)_2$ compared with Co foil, and α-$Co(OH)_2$.

The oxidation number of Co in the α-$Co(OH)_2$ deposit was then evaluated using XAS. The XAS characteristic of the as-electrodeposited α-$Co(OH)_2$ is in good agreement with that of the α-$Co(OH)_2$ standard, not Co metal foil (see Fig. 3d). As the result, it can be concluded that the oxidation number of Co in the α-$Co(OH)_2$ structure is 2+. Thermal stability of the as-prepared α-$Co(OH)_2$ was also studied. Fig. S4 of ESI shows the TGA and its derivative pattern of the as-scrapped α-$Co(OH)_2$ carried out in the temperature range 30-350 ºC in O_2 gas for which its weight loss undergoes two steps. The first one at 86 ºC is due to the dehydration of adsorbed water inside the interlayers.[25] The second weight loss at 211 ºC is owing to the decomposition of $Co(OH)_2$ providing Co_3O_4.[26]

3.2 Electrochemical evaluation

Fig. 4a and b show cyclic voltammograms (CVs) of the α-$Co(OH)_2$/rGO/CFP electrode produced by the chronoamperometry at -0.5 V vs. Ag/AgCl for 10 min and tested in 1-6 M NaOH and KOH. The charge/discharge storage mechanism is clearly observed from the sharp redox peaks observed in CVs (see Fig. 4a and b). Based on the CV results with an oxidation peak in the forward scan and a reduction peak in the backward scan, the mechanism is proposed as following redox reaction (3);

$$Co(OH)_2 + OH^- \leftrightarrows CoOOH + H_2O + e^- \quad (3)$$

There is no subsequent oxidation reaction leading to very stable phase CoO_2 as previously reported.[27] In addition to the sharp redox peaks observed, the peak separation is about 0.1-0.2 V indicating that the as-electrodeposited α-$Co(OH)_2$ behaves as the redox-based electrode.[28] It is necessary to note here that there is no sharp redox peak for two well-known pseudocapacitor materials e.g. MnO_2 and RuO_2, which store charges via the surface redox reactions.[29, 30]

For the effect of the electrolytes and their concentrations, CVs in Fig. 4a and b show that the current densities of the α-$Co(OH)_2$/rGO/CFP tested in both 1 M NaOH and KOH are much higher than those evaluated in 2-6 M NaOH and KOH. A potential range achieved in this work is also wider than that (–0.1 to 0.45 V) previously reported.[31] At the potential over 0.55 V vs. Ag/AgCl, the oxygen evolution reaction occurs. Further observation, there is no significant difference in the current density obtained from 1 M NaOH and 1 M KOH. These results are somewhat interesting since other previous works mainly used KOH at high concentrations e.g. 6 M KOH.[32, 33] At high concentrations, the stripping (dissolution) of the deposits was also observed for which the colour of the electrolytes turned from no colour to light brown during the charging/discharging especially at fast charge/discharge rates. For further confirmation, the electrochemical impedance spectroscopy was also carried out. Nyquist plots, measured in NaOH and KOH using a sinusoidal signal of 40 mV over the frequency range from 100 kHz to 1 mHz in Fig. 4c and d, show that NaOH and KOH at high concentrations (3-6 M) are rather corrosive since clear semi-circles at high frequency (the lower left portion of the plots) relating to the stripping of metal hydroxide are observed.

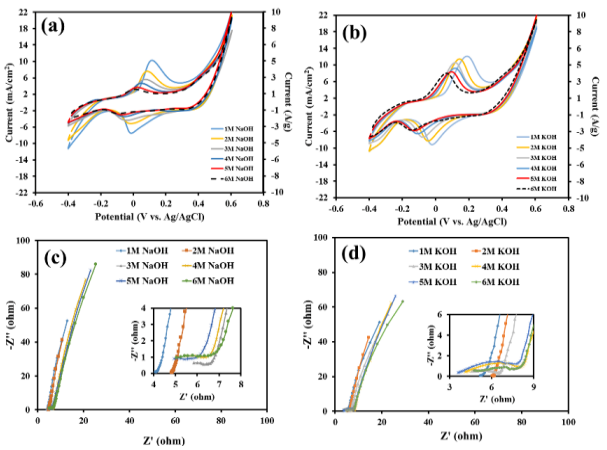

Fig. 4 Cyclic voltammograms of α-$Co(OH)_2$/rGO/CFP electrodes in (a) NaOH and (b) KOH at different concentrations at a scan rate of 10 mV s^{-1} as well as Nyquist plots of α-$Co(OH)_2$/rGO/CFP electrodes in (c) NaOH and (d) KOH at different concentrations (1-6 M) at 0.2 V vs. Ag/AgCl.

SEM images of all electrodes after tested in 1-6 M NaOH and KOH are shown in Fig. S5 and S6, respectively. Clearly, the strong basic electrolytes (3-6 M NaOH and KOH) can deform the porous structure of the α-$Co(OH)_2$ becoming denser, which is not good for the electrolyte diffusion. NaOH is also commercially 2-fold cheaper than KOH. As the results, 1 M NaOH was then used as the electrolyte in the electrochemical evaluation hereafter.

The effect of the electrodeposition time to the areal-based charge storage performance of α-$Co(OH)_2$/rGO/CFP was investigated. The weights of α-$Co(OH)_2$ on 1-cm^2 rGO/CFP electrodes produced for 1, 2, 5, 10, 20, and 40 min are ca. 0.1, 0.2, 0.8, 2.2, 2.7, and 4.7 mg, respectively. The capacitance (*C*) was calculated from the CV by following eq. (4) where *I* is a discharging current

(A), t is discharging time (s), and ΔV is the working potential range (ca. 0.8 V);

$$C = \int \frac{Idt}{\Delta V} \quad (4)$$

The areal capacitance (C_a) can be calculated by dividing C with the geometrical surface area of the electrode.[34] The areal capacity (mAh cm^{-2}) is calculated by multiplying C_a (F cm^{-2}) with $\Delta V/3.6$.[34] C_a and areal capacity values of all as-fabricated electrodes at different loading contents vs. a square root of scan rates are shown in Fig. 5a for which these values are decreased as a function of square root of the scan rate indicating that the charge storage mechanism is under diffusion limit. This is a characteristic of redox-based energy storages.[1, 2, 35, 36] The 2.2-mg α-Co(OH)$_2$/rGO /CFP produced for 10 min can provide the C_a of 2.2 F cm^{-2} and the areal capacity of 6.2 mAh cm^{-2} at a scan rate of 2 mV s^{-1}. These two values are much higher than those produced at other deposition time and those of other materials previously reported.[34, 37-39] At high loading content of α-Co(OH)$_2$, the C_a and areal capacity values are limited by the poor conductivity of α-Co(OH)$_2$.[37] At low loading content of α-Co(OH)$_2$, EDLC, contributed by the rGO, plays a major role but faradaic current is rather low leading to low C_a and areal capacity. This is because α-Co(OH)$_2$ did not cover the whole rGO/CFP surface (see Fig. S3a-c of ESI).

To further investigate the charge storage mechanism, the as-scrapped α-Co(OH)$_2$ was mixed with conductive carbon black and PVDF binder in N-methyl-2-pyrrolidone solvent at the weight ratio of 80:10:10 wt.% (α-Co(OH)$_2$:PVDF:carbon black). The mixture was then casted on the rGO/CFP electrode and vacuum dried at 60 ºC overnight. The CV results, carried out in 1 M NaOH at a scan rate of 1 mV s^{-1} (Fig. 5b), show that increasing the mass loading content of α-Co(OH)$_2$ from 1.5 mg to 3.0 mg provides no significant difference in the peak position and area as well as faradaic current related to the redox reaction (3) of α-Co(OH)$_2$. However, the C_a of the as-fabricated electrodes is rather low about 0.16 F cm^{-2} when compared with 2.2 F cm^{-2} achieved by the electrodeposition method.

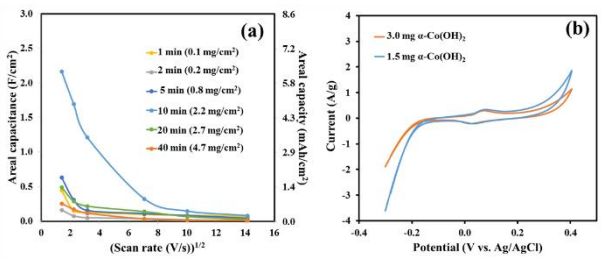

Fig. 5 (a) Areal capacitance (F cm^{-2}) and areal capacity (mAh cm^{-2}) vs. a square root of the scan rates and (b) cyclic voltammograms of the electrodes fabricated from as-scrapped α-Co(OH)$_2$ mixed with PVDF and carbon black at the weight ratio of 80:10:10 in 1 M NaOH at a scan rate 1 mV s^{-1}.

The specific capacitance of the 10-min α-Co(OH)$_2$/rGO/CFP finely tuned was also investigated by the galvanostatic charge-discharge at different applied specific currents (1.8-9.1 A/g) as shown in Fig. 6a. For the charging process, a linear variation of the time dependence at the potential (below about 0.08 V vs. Ag/AgCl) indicates pure EDLC behavior. Whilst, a slope variation of the time dependence at the potential range of ca. 0.08–0.20 V vs. Ag/AgCl exhibits a typical pseudocapacitance characteristic due to the oxidation reaction of Co(OH)$_2$ (see forward reaction 3). For the discharging process, the potential of ca. -0.1 V vs. Ag/AgCl indicates the reduction reaction of CoOOH (see backward reaction 3). The specific C values of the electrode calculated by following equation; $C = I\Delta t/\Delta V$ where I is applied specific current, Δt is discharging time, and ΔV is working potential excluding iR drop, are 1096, 1076, 1060, 1044, and 1022 F g^{-1} at 1.8, 2.7, 3.6, 4.5 and 6.8 A g^{-1}, respectively. For the relative comparison to other previous reports related to the Co(OH)$_2$ supercapacitor electrodes, the specific capacitance of the 10-min α-Co(OH)$_2$/rGO/CFP obtained in this work was also calculated and listed in Table 1. In addition, the capacity retention of the as-fabricated electrode was investigated by the galvanostatic charge-discharge in 1 M NaOH at 1.8 A g^{-1} over 5000 cycles (see Fig. S7 of the supporting information). The capacity retention is still rather high about 98% over 5000 consecutive cycles (see Fig. 6b).

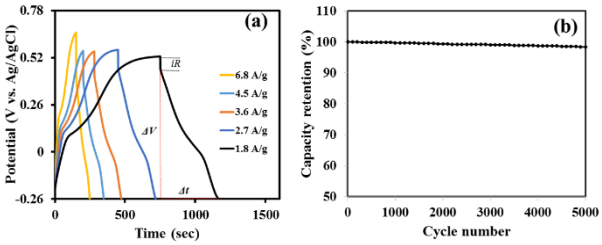

Fig. 6 (a) Charge-discharge curves of 10-min α-Co(OH)$_2$/ rGO/CFP in 1 M NaOH at different applied specific currents and (b) its capacity retention over 5000 cycles.

Table 1. The specific capacitances of Co(OH)$_2$-based supercapacitor electrodes tested in different concentrations of alkaline electrolytes.

Materials	Electrolytes	Testing methods and conditions	Specific capacitance (F g^{-1})	Refs
Co(OH)$_2$ nanosheets	6 M KOH	C/D[a] at 0.83 A g^{-1}	1083	32
Co(OH)$_2$ flakes on 3D multi-layered graphene foam	1M KOH	C/D at 9.09 A g^{-1}	1030	14
Co(OH)$_2$ nanoparticles	2 M KOH	C/D at 1 A g^{-1}	474	21
Co(OH)$_2$ nanosheets	1 M KOH	C/D at 1 A g^{-1}	840	40
Whisker-like Co(OH)$_2$	2 M KOH	C/D at ca. 1.3 A g^{-1}	325	41
Co(OH)$_2$ nanosheets	1 M KOH	C/D at 2 A g^{-1}	651	42
Flower-like Co(OH)$_2$	3 M KOH	C/D at 1.3 A g^{-1}	434	43
Co(OH)$_2$ nanocone	2 M KOH	C/D at 2 A g^{-1}	562	44
Co(OH)$_2$ flakes	1 M KOH	C/D at 2A g^{-1}	693.8	45
Co(OH)$_2$//Co(OH)$_2$ device	1 M KOH	CV at 5 mV s^{-1}	44	46
Co(OH)$_2$ nanosheets	1 M Na_2SO_4	CV at 8 mV s-1	141	47
Co(OH)$_2$ nanowires	6M KOH	C/D at 0.5 A g-1	358	33

Materials	Electrolytes	Testing methods and conditions	Specific capacitance ($F\ g^{-1}$)	Refs
Flower-like $Co(OH)_2$	3M KOH	C/D at 0.5 μA g-1	170	[48]
$Co(OH)_2$ nanocone arrays	2 M KOH	C/D at 2 A g^{-1}	562	[44]
Mesoporous $Co(OH)_2$	1 M KOH	CV[b] at 5 mV s^{-1}	246.7	[49]
α-$Co(OH)_2$ nanosheets/rGO/CFP	1 M NaOH	C/D at 1.8 A g^{-1}	1096	This work

[a]C/D is a galvanostatic charge/discharge and [b]CV is a cyclic voltammetry.

4. Conclusions

α-$Co(OH)_2$ nanosheets were electrodeposited on the rGO/CFP using a simple chronoamperometry method at an applied potential of -0.5 V vs. Ag/AgCl for 10 min. The mass loading content of α-$Co(OH)_2$ on the rGO/CFP is about 2.2 mg cm^{-2}. The as-fabricated electrode was electrochemically tested in 1-6 M NaOH and KOH. It was found that the alkaline electrolytes at high concentrations i.e., 3-6 M KOH and NaOH can strip off and/or deform the porous struture of the α-$Co(OH)_2$ deposit. 1 M [OH^{-1}] is a proper concentration providing high charge storage performance without the structural deformation of porous α-$Co(OH)_2$ LDH. The α-$Co(OH)_2$/rGO/CFP provides high specific capacitance of 1096 F g^{-1} at 1.8 A g^{-1} due to a synergic effect of rGO storing ionic charges via EDLC and α-$Co(OH)_2$ storing electron via the redox reaction. The capacity retention of the electrode is about 98% after testing 1 M NaOH with 5000 consecutive charge/discharge cycles.

Acknowledgment

This work was financially supported by the Thailand Research Fund (TRF) and the Commission on Higher Education (TRG5680043). Supports from the TRF Senior Research Scholar (RTA560008), the Kasetsart University Research and Development Institute (KURDI), National Research University Project of Thailand (NRU), and National Nanotechnology Center (NANOTEC) under the National Science and Technology Development Agency are also acknowledged.

Notes and references

[a] National Center of Excellence for Petroleum, Petrochemicals and Advance Material, Department of Chemical Engineering, Faculty of Engineering, Kasetsart University, Bangkok 10900, Thailand. *Fax: +66(0)2-561-4621; Tel:+66(0)2-942-8555; E-mail: fengmrs@ku.ac.th*

[b] *Center for Advanced Studies in Nanotechnology and Its Applications in Chemical, Food and Agricultural Industries, Kasetsart University, Bangkok 10900, Thailand*

** Corresponding author: M. Sawangphruk*
Tel: +66(0)2-942-8555 Fax: +66(0)2-561-4621. E-mail: fengmrs@ku.ac.th

† Electronic Supplementary Information (ESI) available: Morphological characterizations, TGA, electrochemical evaluation, can be seen in ESI. See DOI: 10.1039/b000000x/

1. P. Simon and Y. Gogotsi, *Nat. Mater.*, 2008, **7**, 845-854.
2. Y. Gogotsi, *Nature*, 2014, **509**, 568-570.
3. N. Devillers, S. Jemei, M.-C. Péra, D. Bienaimé and F. Gustin, *J. Power Sources*, 2014, **246**, 596-608.
4. E. L. Schneider, C. T. Oliveira, R. M. Brito and C. F. Malfatti, *J. Power Sources*, 2014, **262**, 1-9.
5. C. Liu, Z. Yu, D. Neff, A. Zhamu and B. Z. Jang, *Nano Lett.*, 2010, **10**, 4863-4868.
6. J. Hu, Z. Kang, F. Li and X. Huang, *Carbon*, 2014, **67**, 221-229.
7. M. F. El-Kady, V. Strong, S. Dubin and R. B. Kaner, *Science*, 2012, **335**, 1326-1330.
8. H. Chen, L. Hu, M. Chen, Y. Yan and L. Wu, *Adv. Funct. Mater.*, 2014, **24**, 934-942.
9. Y. Tang, Y. Liu, S. Yu, S. Mu, S. Xiao, Y. Zhao and F. Gao, *J. Power Sources*, 2014, **256**, 160-169.
10. G. Chen, S. S. Liaw, B. Li, Y. Xu, M. Dunwell, S. Deng, H. Fan and H. Luo, *J. Power Sources*, 2014, **251**, 338-343.
11. S. Faraji and F. N. Ani, *J. Power Sources*, 2014, **263**, 338-360.
12. A. D. Jagadale, V. S. Kumbhar, D. S. Dhawale and C. D. Lokhande, *Electrochim. Acta*, 2013, **98**, 32-38.
13. W.-J. Zhou, D.-D. Zhao, M.-W. Xu, C.-L. Xu and H.-L. Li, *Electrochim. Acta*, 2008, **53**, 7210-7219.
14. U. M. Patil, M. S. Nam, J. S. Sohn, S. B. Kulkarni, R. Shin, S. Kang, S. Lee, J. H. Kim and S. C. Jun, *J. Mater. Chem. A*, 2014. doi: 10.1039/C4TA03953J.
15. M. Sawangphruk, A. Krittayavathananon, N. Chinwipas, P. Srimuk, T. Vatanatham, S. Limtrakul and J. S. Foord, *Fuel Cells*, 2013.
16. M. Sawangphruk, P. Srimuk, P. Chiochan, A. Krittayavathananon, S. Luanwuthi and J. Limtrakul, *Carbon*, 2013, **60**, 109-116.
17. M. Sawangphruk, P. Srimuk, P. Chiochan, T. Sangsri and P. Siwayaprahm, *Carbon*, 2012, **50**, 5156-5161.
18. Y. Sanguansak, P. Srimuk, A. Krittayavathananon, S. Luanwuthi, N. Chinvipas, P. Chiochan, J. Khuntilo, P. Klunbud, T. Mungcharoen and M. Sawangphruk, *Carbon*, 2014, **68**, 662-669.
19. V. Gupta, T. Kusahara, H. Toyama, S. Gupta and N. Miura, *Electrochem. Commun.*, 2007, **9**, 2315-2319.
20. Z. Wu, X.-L. Huang, Z.-L. Wang, J.-J. Xu, H.-G. Wang and X.-B. Zhang, *Sci. Rep.*, 2014, **4**. doi:10.1038/srep03669.
21. Z. Li, J. Wang, L. Niu, J. Sun, P. Gong, W. Hong, L. Ma and S. Yang, *J. Power Sources*, 2014, **245**, 224-231.
22. Z. Liu, R. Ma, M. Osada, K. Takada and T. Sasaki, *J. Am. Chem. Soc.*, 2005, **127**, 13869-13874.
23. J. Yang, H. Liu, W. N. Martens and R. L. Frost, *J. Phys. Chem. C*, 2009, **114**, 111-119.
24. N. S. McIntyre and M. G. Cook, *Anal. Chem.*, 1975, **47**, 2208-2213.
25. Y. Zhu, H. Li, Y. Koltypin and A. Gedanken, *J. Mater. Chem.*, 2002, **12**, 729-733.
26. R. S. Jayashree and P. Vishnu Kamath, *J. Mater. Chem.*, 1999, **9**, 961-963.
27. X. Wang, C. Yan, A. Sumboja, J. Yan and P. S. Lee, *Adv. Energy Mater.*, 2014, **4**, n/a-n/a.
28. P. Simon, Y. Gogotsi and B. Dunn, *Science*, 2014, **343**, 1210-1211.
29. H. Y. Lee and J. B. Goodenough, *J. Solid State Chem.*, 1999, **144**, 220-223.
30. V. Subramanian, S. C. Hall, P. H. Smith and B. Rambabu, *Solid State Ionics*, 2004, **175**, 511-515.

31. W. J. Zhou, J. Zhang, T. Xue, D. D. Zhao and H. L. Li, *J. Mater. Chem.*, 2008, **18**, 905-910.
32. J. Zhang, X. Wang, J. Ma, S. Liu and X. Yi, *Electrochim. Acta*, 2013, **104**, 110-116.
33. Y. Tang, Y. Liu, S. Yu, S. Mu, S. Xiao, Y. Zhao and F. Gao, *J. Power Sources*, 2014, **256**, 160-169.
34. K. Jost, G. Dion and Y. Gogotsi, *J. Mater. Chem. A*, 2014**, 2**, 10776-10787.
35. M. Toupin, T. Brousse and D. Bélanger, *Chem. Mater.*, 2004, **16**, 3184-3190.
36. B. E. Conway, *J. Electrochem. Soc.*, 1991, **138**, 1539-1548.
37. D. Ghosh, S. Giri and C. K. Das, *ACS Sus. Chem. Eng.*, 2013, **1**, 1135-1142.
38. X. Wang, S. Liu, H. Wang, F. Tu, D. Fang and Y. Li, *J. Solid State Electrochem.*, 2012, **16**, 3593-3602.
39. L. Mai, H. Li, Y. Zhao, L. Xu, X. Xu, Y. Luo, Z. Zhang, W. Ke, C. Niu and Q. Zhang, *Sci. Rep.*, 2013, **3**. doi:10.1038/srep01718.
40. V. Gupta, S. Gupta and N. Miura, *J. Power Sources*, 2008, **177**, 685-689.
41. C. Yuan, L. Hou, L. Shen, D. Li, F. Zhang, C. Fan, J. Li and X. Zhang, *Electrochim. Acta*, 2010, **56**, 115-121.
42. T. Zhao, H. Jiang and J. Ma, *J. Power Sources*, 2011, **196**, 860-864.
43. C. Yuan, L. Yang, L. Hou, D. Li, L. Shen, F. Zhang and X. Zhang, *J. Solid State Electrochemi.*, 2012, **16**, 1519-1525.
44. F. Cao, G. X. Pan, P. S. Tang and H. F. Chen, *J. Power Sources*, 2012, **216**, 395-399.
45. C. Zhao, X. Wang, S. Wang, Y. Wang, Y. Zhao and W. Zheng, *Int. J. Hydrogen Energy*, 2012, **37**, 11846-11852.
46. A. D. Jagadale, V. S. Kumbhar, D. S. Dhawale and C. D. Lokhande, *Electrochim. Acta*, 2013, **98**, 32-38.
47. F. S. Fedorov, J. Linnemann, K. Tschulik, L. Giebeler, M. Uhlemann and A. Gebert, *Electrochim. Acta*, 2013, **90**, 166-170.
48. X. Ji, P. M. Hallam, S. M. Houssein, R. Kadara, L. Lang and C. E. Banks, *RSC Advances*, 2012, **2**, 1508-1515.
49. J. M. Ko, D. Soundarajan, J. H. Park, S. D. Yang, S. W. Kim, K. M. Kim and K.-H. Yu, *Cur. App. Phys.* 2012, **12**, 341-345.